CHAPTER 2

Experimental Section

2.1. Introduction

This chapter deals with the method of preparation of electrodes, electrode pre-treatment procedures and electrochemical cell arrangements for the experimental setup in a detailed manner. The various experimental techniques and their working principles used in our experimental work of this thesis have also been explained. Several techniques such as electrochemical, surface, microscopic and diffraction techniques have been used for the study. The electrochemical techniques vary from electrodeposition, cyclic voltammetry (CV), electrochemical impedance spectroscopy (EIS), stripping voltammetry, chronopotentiometry (CP) and Tafel plot analysis were used. Surface analytical techniques namely Grazing angle FTIR spectroscopy have been used for the characterization of self-assembled monolayer (SAM) on Au surface and X-ray diffraction studies have been carried out essentially to characterize the different self aggregated structural phases formed by the surfactant molecules and to determine the average particle size of the metal particles obtained from the template electrodeposition. The microscopic techniques such as scanning electron microscopy (SEM) and scanning tunneling microscopy (STM) were performed to characterize the surface topography and morphology of the modified surfaces. Polarizing light microscopy studies were carried out mainly to confirm the different textural structures formed by the various phases produced by the self-assembly of surfactants. The working principle and the experimental setup used for all the experimental techniques have been elaborately explained below.

2.2. Electrochemical cell

For performing the electrochemical experiments, a conventional three-electrode electrochemical cell was used. The cell is made up of glass with a Teflon lid machined to fit with the B-55 size neck. The lid was made in such a way that it could accommodate the working, counter and reference electrodes. In addition it also has the provision of inlet and outlet to allow the flow of inert gas to deaerate the cell containing the electrolytic solution. All the electrodes were fitted with a ground joint of size B-14 to use in the cell arrangement. The counter electrode is a platinum foil of large surface area, which was sealed to a glass tube. The reference electrode is a saturated calomel electrode (SCE) with a luggin capillary that can be kept very close to the working electrode to minimize the iR drop. The aqueous KCl solution in the reference electrode was replaced very frequently in order to keep the electrode fresh and to avoid any fluctuation in the potential values. The working electrode was held by an electrode holder, which is a long gold plated brass rod with a slot at one end where the working electrode was held using screws. This sample holder was fixed to a Teflon B-14 cone that was fixed to the socket of the central ground joint. For the experiments involving non-aqueous solvents, an electrochemical cell having a separate compartment for the reference electrode to be kept was used which has been connected to the main cell through a glass tube with a stop cork in order to prevent mixing of electrolytic solution. Before each experiment, the cell was washed with soap powder and then thoroughly flushed with free flowing water and finally rinsed in distilled water and kept in a hot air oven at 100^0C for at least 1 hour before the start of the experiment.

In the case of template electrodeposition technique, a conventional two-electrode experimental setup with anode and cathode containing the metal

salts of the corresponding metal to be deposited on the cathode material along with the template present in the electrolytic solution was used.

2.3. Electrodes

In our study, either the evaporated gold sample with predominantly Au(111) orientation or a polycrystalline gold/platinum wire (disc) electrode was used as a working electrode. A platinum foil of large surface area was used as a counter electrode. A saturated calomel electrode (SCE) was used as a reference electrode in the aqueous medium whereas a silver rod was used as a quasi-reference electrode in the experiments involving non-aqueous solvents. This electrode has a stable potential and is also free from any liquid junction potential. The nickel electrodes obtained from the template electrodeposition were used as strips for the evaluation and characterization as a working electrode. In the case of study of electron transfer kinetics using surfactants self-aggregated systems as electrolytes, a platinum working electrode was used in the form of a foil or a disc.

2.4. Preparation of working electrode

In most of our electrochemical studies, gold and platinum electrodes were used as working electrodes. All the working electrodes used for the experimental studies were designed and fabricated in our laboratory. The gold disk electrode was fabricated by proper sealing of a 99.99% pure gold wire (obtained from Arora Mathey, Kolkata, India) of 0.5mm diameter with the soda lime glass having the thermal expansion coefficient close to that of gold. A similar procedure was followed to obtain the disc shaped platinum electrode. All these electrodes show no leakage when kept in electrolytes for long periods indicating an excellent metal-glass sealing. Nickel strips used in the

electrodeposition technique were obtained using electroforming procedure. The electroforming of nickel was carried out on stainless steel cathode material using sulphurized bars of nickel as anode from nickel sulphamate bath at a current density of 10-15 mA/cm^2. Superglue or araldite was applied on the electrode to expose only a well-defined geometric area of the working electrode for the experiments and the remaining portion of the electrode was covered using parafilm (a fluoropolymer) and Teflon tape to prevent any chemical attack on the resin.

2.5. Electrode pre-treatment procedure

In this section, different surface pre-treatment procedures used for the polycrystalline samples are described. We have carried out two different methods for the surface pre-treatment namely mechanical polishing and chemical etching, which are described below.

2.5.1. Mechanical polishing

The disc shaped wire (0.5mm diameter) electrodes of gold and platinum of purity >99.9% were used as the working electrodes. Immediately before the start of the experiments, the electrodes were hand polished with emery papers of grade 800 and 1000 followed by polishing in aqueous slurries of progressively finer alumina powder (Buehler) of size varying from 1.0μm, 0.3μm and 0.05μm on a microcloth. Then the electrodes were ultrasonically cleaned in distilled water to remove alumina particles and finally cleaned with millipore water. In the case of template electrodeposition, the nickel strips obtained using electroforming were also pre-treated using a similar procedure before carrying out the deposition process.

2.5.2. Chemical etching

On using the wire/disc electrodes of gold and platinum, all the working electrodes were polished with alumina powder and ultrasonicated in distilled water (as described in the previous section) before chemical etching. The gold electrodes were chemically etched using either dilute aqua regia solution containing concentrated HCl, concentrated HNO_3 and water in 3:1:4 ratio or "piranha" solution which is a mixture of 30% H_2O_2 and concentrated H_2SO_4 in 1:3 ratio. (_Caution: The usage of "piranha" solution is very dangerous and injurious to health. A care should be taken on handling this solution and it should not be exposed to any chemical reagents and reactive compounds and the contact of this solution with any parts of human body especially to that of eye should also be avoided._) For using the evaporated gold strips as working electrodes, the surface pre-treatment was carried out using either dilute aqua region or piranha solution by keeping the electrode for about 1-2 minutes. This procedure had been shown to yield a substrate with the best blocking properties for the self-assembled monolayer formation of alkanethiols on gold [1,2]. Before SAM formation, the electrodes were thoroughly washed with distilled water followed by rinsing in millipore water. In the case of platinum electrodes, after polishing in emery paper and alumina powder, it was chemically etched with concentrated HNO_3 for about 1-2 minutes. Before introducing into the cell, after the chemical etching, the electrodes were cleaned thoroughly in distilled water and followed by rinsing in millipore water. Similarly for nickel strips, before deposition the strips were chemically etched with concentrated HCl and water in 1:1 ratio for about 1-2 minutes immediately after the mechanical polishing. These surface pre-treatment procedures not only clean the surface by removing the unwanted physisorbed species but also chemically etch the

surface to initiate the reactions such as deposition of metals and adsorption of molecules on these surfaces.

2.6. Preparation of evaporated gold sample

The evaporated gold samples were used as strips mainly for electrochemical, microscopic and Grazing angle FTIR spectroscopic techniques used for the characterization studies. Evaporation of gold on glass was carried out in a vacuum evaporation unit (Hindhivac) at a pressure of 2 x 10^{-5} mbar. Chromium underlayers of approximately 2-5nm in thickness were deposited on glass before the gold evaporation in order to improve the adhesion of gold on glass. The substrate temperature was maintained at 350^{0}C throughout during the deposition process. The resistive evaporation of gold was carried out at a rate of 4-5Å sec^{-1}. The final thickness of the gold film was calculated to be about 100 nm. This procedure normally yields a gold substrate with predominantly (111) crystallographic orientation [3], which was confirmed by X-ray diffraction studies. As described earlier, only a small portion with well-defined geometric area of the sample was exposed to the electrolytic solution for the analysis.

In this section, the experimental setup along with the electrode preparation and surface pre-treatment procedures were described elaborately. The corresponding experimental procedures performed for different systems in this thesis work were presented in the experimental sections of the respective chapters.

2.7. Experimental techniques and their working principle

We have used a variety of experimental techniques in the course of our investigation and this section deals with those experimental techniques and their working principles. We have used several electrochemical, spectroscopic and

microscopic techniques in this thesis work. Electrochemical techniques comprise of electrodeposition, cyclic voltammetry (CV), electrochemical impedance spectroscopy (EIS), stripping voltammetry, chronopotentiometry and Tafel plot analysis that have been extensively used in this study. The microscopic techniques such as scanning electron microscopy (SEM) and scanning tunneling microscopy (STM) have been carried out essentially to characterize the surface morphology and topography, while the polarizing light microscopy was used to study the textural characteristics of the different phases formed by the self-assembly of surfactants. Apart from these techniques, we have also used Grazing angle FTIR spectroscopy and X-ray diffraction studies in this work.

2.7.1. Electrodeposition

Electrodeposition is a process of depositing metals or metal oxides on a surface essentially to modify it for possessing certain desired properties [4]. It is mainly applied to alter the characteristics of a surface so as to provide improved appearance, ability to withstand corrosive agents, resistance to abrasion, decoration of the surface or a combination of them, although it is used simply to alter the dimensions. The process of electrodeposition occurs by means of electrolysis. A typical electrolysis cell consists of an anode, normally the metal to be deposited and cathode onto which the metal is deposited with an electrolyte containing the aqueous solution of the metal salt. Anode is an electrode where oxidation takes place while at cathode reduction occurs. On applying the current to the cell, the deposition starts occurring at cathode by the electron transfer process. The dissolution of an ion at the anode is accompanied by deposition of an ion at the cathode.

There are two kinds of deposition namely electroplating and electroless plating. In electroplating the deposition occurs by the application of current, while in the other process of electroless plating the deposition is based on the chemical reactions using the catalyst without applying any current. In our work, we have carried out experiments mainly based on the process of electroplating and the growth of metal deposit and various parameters involved in electroplating have been explained in the following section.

Growth of deposits

During the process of electrodeposition, the metal atoms are not deposited as continuous sheets from one edge of the cathode to the other. The metal ions attached to the cathode only at certain favoured sites especially at the defects, by losing some of the water or other ligands, which were previously attached to them [5,6]. This process leads to a bond formation between the metal ion and the cathode surface. These adions diffuse over the surface to kinks, edges, steps or other irregularities where they have been incorporated into the metal lattice. As these growth sites travel across the crystal face, monoatomic growth layers bounded by microsteps are produced. Further growth occurs to form the stacks of multilayer. The microsteps present originally at the emergence of points of screw dislocations or at other defects and they are formed by two dimensional nucleation facilitated by the presence of impurities. Lateral growth proceeds from various centers until the neighboring lattices form a boundary at the lines of contact. Using this process, the symmetrical crystal faces are not developed and only the individual structures called as grains are produced.

The faradaic efficiency is an important parameter, which quantifies the amount of deposition. It is defined as the ratio of the weight of metal actually

deposited to the corresponding weight, which would have deposited if all the current had been used for the metal deposition. A high faradaic efficiency is desirable in choosing the correct composition for the electroplating bath. During deposition, the mass transport is governed by three processes namely diffusion, convection and migration. There are several parameters such as pH, temperature, bath composition, current density, inhibitors and brightening agents that can affect the structure of a metal deposit and one should take care of all these parameters to obtain a very good deposit with desirable properties.

In our studies, we have mainly used electroplating technique to carry out the experiments of template electrodeposition of nickel, which has been explained and discussed in chapter 3 elaborately.

2.7.2. Cyclic voltammetry (CV)

Cyclic voltammetry commonly known as "CV" is a very much popular and most extensively used electrochemical technique among the potential sweep techniques. The simplest of potential sweep techniques is linear sweep voltammetry (LSV), which involves sweeping the electrode potential between the limits E_1 and E_2 at a known sweep rate v, before halting the potential sweep. In the case of cyclic voltammetry (CV) the waveform applied initially is same as LSV, but on reaching the potential E_2 the sweep is reversed usually at the same scan rate as the forward sweep instead of terminating the scan. Typical potential-time profile for CV is shown in figure 1.
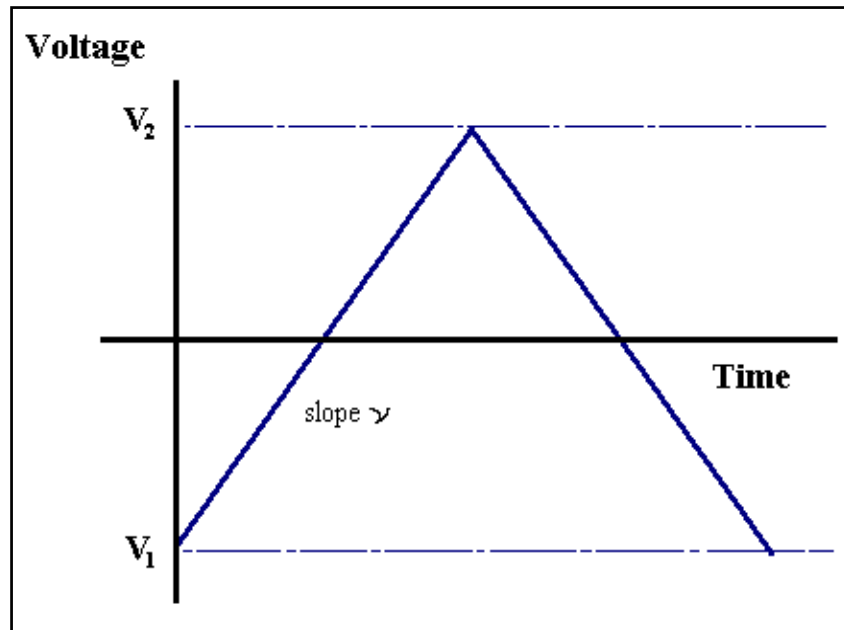
Figure 1: Potential-Time profile for cyclic voltammetry

Cyclic voltammetry concerns with the scanning of working electrode potential between the potential limits of V_1 and V_2 at a known scan rate ν, in both the forward and reverse direction and measuring the current of the electrochemical cell. The resultant current of the system involves the faradaic current due to the various electrochemical phenomenon occurring on the electrode surface such as electron transfer redox reactions and adsorption processes in addition to the capacitive current due to the double layer charging at these potentials [7,8]. A plot of measured current as a function of applied potential is known as "cyclic voltammogram". It is an electrochemical spectrum indicating the potentials at which several processes occur can be obtained rapidly and from the dependence of current on the sweep rate, the involvement of coupled homogenous reactions and the process like adsorption can also be recognized. Apart from these, the kinetic parameters and the mechanism of

different heterogeneous reactions occurring on the electrode surface can also be determined. The conventional experiments of recording voltammograms use a range of sweep rates vary from few mV/s to few hundred V/s and for several values of V_1 and V_2. Usually there will be several peaks and by observing the characteristics of these peaks over the potential limits and as a function of scan rates, it is possible to determine and conclude how the processes represented by the peaks are related. By noting the difference between the first and subsequent cycles resulting in the cyclic voltammograms, a detailed mechanistic information about the electrochemical reactions can be derived. Normally the shape of the cyclic voltammogram depends on the type of redox reactions. Figure 2 shows a typical cyclic voltammogram for a single electron reversible process.
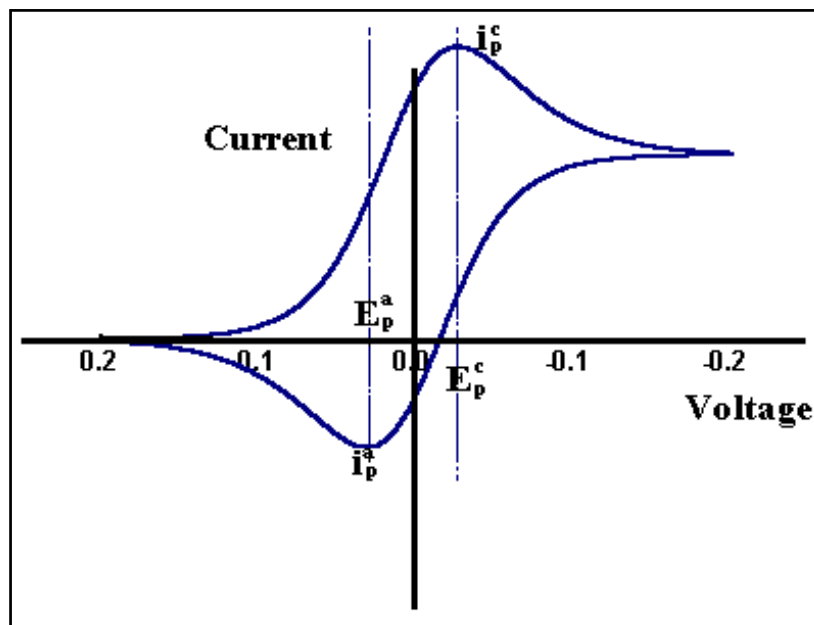

Figure 2: Cyclic voltammogram for a single electron reversible process

For a typical single electron reversible redox reaction of the type,

$$O + ne^- \rightleftharpoons R$$

the rate of charge transfer is always greater than the rate of mass transfer at all potentials and the redox reaction is under diffusion control. The ratio of concentrations of oxidant and reductant species of a reversible reaction is given by Nernst equation and a concentration gradient exists within the region near the electrode surface known as Nernst diffusion layer, where the concentration gradient of the electroactive species is linear. Also the Nernstian equilibrium is always maintained at the electrode surface and at all the potentials. The shape of current-potential profile for a one-electron reversible redox reaction as shown in figure 2 can be understood in the following way. When the potential of the electrode is made more negative, the surface concentration of the reactant O decreases progressively, thereby the concentration gradient is increased which results in increase in the current. On reaching the electrode potential where O is reduced, the surface concentration of O decreases from its bulk value in order to satisfy the Nernst equation and the concentration gradient is setup. As a result a current proportional to the concentration gradient at the electrode surface flows. Due to diffusion of ions, the concentration gradient does not remain constant and it started to decrease. At the same time, the electrode potential is also continuously changing leading to a further decrease of surface concentration of O until it effectively reaches to zero concentration. Once the concentration of O reaches zero, the gradient decreases due to the accumulation of reduced species R, in the vicinity of the electrode surface (relaxation effect) and hence the current flow also decreases. Overall, this behaviour gives rise to a peak shaped current-potential profile as shown in figure 2. Using similar arguments used for the forward sweep, it can be shown that the current change on reverse sweep also exhibit a peak shaped response

though of the opposite sign. On increasing the sweep rate, the concentration gradient as well as the current results from that also increases due to the shorter time scale of the experiment leading to less relaxation effect.

It can be seen from figure 2 that the cyclic voltammogram for a reversible process shows a minimum charge associated with the anodic process of oxidation compared to that of the cathodic reduction process. This is because throughout the experiment, there is a concentration difference driving R away from the electrode surface resulting in diffusion of most of the product R to the bulk solution and cannot be reoxidised on the time scale of the experiment. The peak current density I_p of the cyclic voltammogram is related to various parameters by the following relationship.

$$I_p = -0.4463 \; nF \; [nF/RT]^{1/2} \; c_o^{\infty} \; D^{1/2} \; v^{1/2}$$

where, I_p is the peak current density in A/cm^2

n is the number of electrons involved in the redox reaction

F is Faraday constant

R is gas constant

T is the absolute temperature

C_o is the concentration of reactant O in mol/cm^3

D is the diffusion coefficient in cm^2/s

v is the sweep rate in V/s

This equation is known as the Randles-Sevick equation and at a temperature of 25^0C this equation reduces to the form given as follows,

$$I_p = -(2.69 \times 10^5) \; n^{3/2} \; c_o^{\infty} \; D^{1/2} \; v^{1/2}$$

From the above equation, it can be noted that the peak current density of the reversible reaction is directly proportional to the concentration of the electroactive species, square root of the diffusion coefficient and also to the square root of the sweep rate. The sign of the current is negative because it is the current for cathodic reaction (as denoted by the convention followed).

A test of reversibility of the electrochemical system is to check whether a plot of I_p as a function of $v^{1/2}$ is both linear and passes through the origin or alternatively (I_p / $v^{1/2}$) is constant. If this is found to be true then further diagnostic tests, which are given below can be applied to verify the reversible nature of the given electrochemical system. For a reversible system the following are the diagnostic tests [8].

1. $\Delta E_p = |E_p^A - E_p^C| = 59/n$ mV
2. $|E_p - E_{p/2}| = 59/n$ mV
3. $|I_p^A / I_p^C| = 1$
4. $I_p \propto v^{1/2}$
5. E_p is independent of v
6. At potentials beyond E_p, $I^{-2} \propto t$

Apart from the reversible system cyclic voltammetry can be used to find out the quasi-reversible and irreversible nature of the electrochemical system. There are also diagnostic tests for these systems to verify the quasi-reversibility and irreversibility of the given system.

Cyclic voltammetry technique has been extensively used in this work to study the electron transfer reactions and to measure the surface area of the electrodes in terms of roughness factor using conventional size macroelectrodes and disk/wire electrodes based on the surfactants self-aggregated systems that exhibit a very low conductivity as the electrolytic media.

2.7.3. Determination of real surface area of metal electrodes

A technique obtained by the slight modification of cyclic voltammetry (based on adsorption/stripping from solution) is very much useful in the determination of real surface area of the metal electrodes. This method is essentially based on hydrogen adsorption from solution in the potential region prior to massive hydrogen evolution and it has been established mainly with Pt, Rh and Ir electrodes [9,10]. The charge under the voltammetric peaks for hydrogen adsorption or desorption (after correcting for the double layer charging current) is assumed to correspond to the adsorption of one hydrogen atom on each metal atom on the surface and is denoted by Q_H. The charge associated with a one to one M-H correspondence per unit surface area represented by, Q^S_H is calculated on the basis of distribution of the metal atoms at the surface. The true surface area in that case is given by,

$$\text{True surface area} = Q_H / Q^S_H$$

In the case of polycrystalline platinum, by assuming that the density of atoms on such a surface is 1.31×10^{15} cm^{-2}, the charge associated with the hydrogen adsorption is 210 μC cm^{-2} [8].

In some other cases, this method is based on the oxygen adsorption resulting in the formation and reduction of monolayer of oxide or hydroxide on the metal surface. Oxygen is assumed to be chemisorbed as a monoatomic layer prior to oxygen evolution with one to one correspondence with the surface metal atoms. In this case the charge associated with the formation or reduction of the oxide layer is given by,

$$Q_0 = 2 \, e \, N_A \, \Gamma_0 \, A$$

where N_A is the Avogadro number, Γ_0 is the surface concentration of atomic oxygen, which is assumed to be equal to N_M, the surface density of metal atoms and A is the area of the electrode. From the value of N_M per unit area, the reference charge value Q_0 can be determined.

The oxide/hydroxide stripping voltammetry is extensively used for gold and nickel electrodes. For polycrystalline gold, the charge corresponds to the desorption of monolayer of gold oxide is 400 $\mu C\ cm^{-2}$ and in the case of nickel, the charge value for the stripping of monolayer of nickel hydroxide is 514 $\mu C\ cm^{-2}$. The true surface area is calculated by measuring the charge of the modified electrodes in acidic or alkaline solution and dividing it by the actual charge value, form which the roughness factor can be determined.

Roughness factor = True surface area / Geometric area

Figure 3 shows the typical cyclic voltammogram of a gold electrode exhibiting the characteristic peaks of gold oxide formation and stripping in perchloric acid solution. The true surface area of gold electrode can be determined by measuring the charge under the gold oxide-stripping peak.
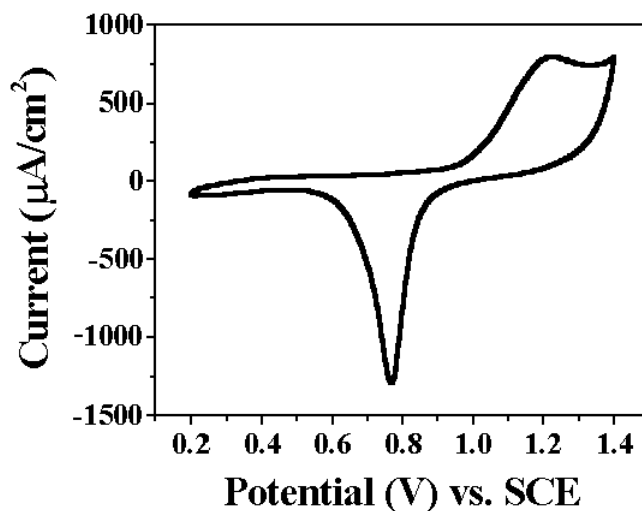

Figure 3: Cyclic voltammogram of a gold electrode in perchloric acid.

In this work, we have used the stripping voltammetry in the case of self-assembled monolayer (SAM) on gold electrodes and template deposited nickel electrodes, essentially to determine the true surface area in terms of roughness factor.

2.7.4. Electrochemical impedance spectroscopy (EIS)

This method comes under the category of ac techniques. In contrast to cyclic voltammetry, which is a dc technique, where the electrochemical system is perturbed far from equilibrium, this method involves the application of a very small perturbation close to the steady state equilibrium. The electrochemical impedance spectroscopy measurements involve essentially a small perturbation of the electrode potential from the equilibrium potential by the application of a sinusoidal signal with 5-10 mV peak-to-peak amplitude and measuring the response of the electrochemical system. Usually, the response to the perturbation, in terms of current differs in phase and amplitude from the applied signal. Figure 4 shows the sinusoidal signals of perturbation and response of the electrochemical system.
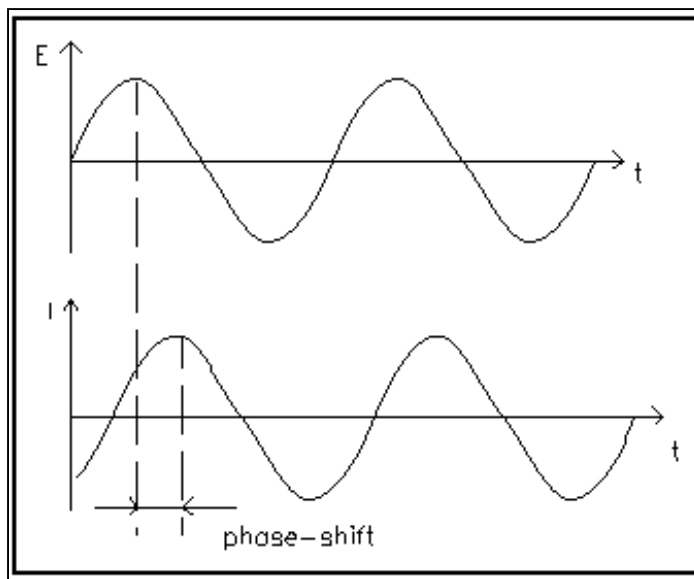

Figure 4: Sinusoidal signal of perturbation and response obtained in EIS

The measurement of phase difference and amplitude (impedance) over a wide range of frequency is very much useful in the analysis of different electrode processes in relation to contributions from double layer charging, diffusion, kinetics, homogeneous and heterogeneous electron transfer reactions and coupled chemical and redox reactions etc. The impedance spectroscopy is extensively used in the study of corrosion, battery, membranes, ionic solids, solid electrolytes, chemically modified electrodes and template deposited porous electrodes etc.

In many of the measurements involving the fast electron transfer reactions, the information has to be obtained at very short times, otherwise diffusion rather than the kinetics becomes the rate determining process. In such a case, the ac techniques are widely used to determine the rate constant for the fast redox reactions. Due to the small perturbation, the system becomes linear and the advantage lies in the ability to treat the response theoretically using the linearized current-potential characteristics. Since, the working region in this method is very close to the equilibrium, the detailed knowledge about the behaviour of current-voltage response over a large range of overpotential is not required. This simplifies the treatment of kinetics and diffusion equations. Using this method, the high precision measurements can be made because the response is indefinitely steady and therefore can be averaged over a long term. Usually, a comparison is made between the electrochemical cell and an equivalent circuit, which contains the combinations of resistances and capacitances that are assumed to behave like a cell. The aim of the impedance measurements is to interpret these equivalent circuits and the values determined using these circuits, in terms of the interfacial phenomena occurring at the electrode | solution interface. The impedance technique is frequently used for

the evaluation of heterogeneous charge transfer parameters and to study the double layer structure.

Principles of AC circuits:

The electrochemical response of a cell to an ac perturbation can be understood by knowing the fundamental principles of ac circuits. If a sinusoidal signal of voltage $V = V_0 \sin \omega t$ is applied to an electrical circuit that contains a combination of resistors and capacitors, the response is a current, which is given by, $I = I_0 \sin (\omega t + \phi)$, where V_0 is the maximum amplitude, I_0 is the maximum current, ω is the angular frequency and ϕ is the phase angle between the perturbation and response. The proportionality factor between V and I is known as the impedance Z. In phasor terms the rotating vectors are separated in the polar diagram by the angle ϕ.

In the case of a pure resistor, R, the phase angle ϕ is zero. According to Ohm's law, $V = IR$, which leads to $I = V_0 \sin \omega t / R$. There is no phase difference between the potential and the current.

For a pure capacitor, C, the current I is given by,

$$I = C \, dV / dt$$

On substituting the value of V as $V_0 \sin \omega t$ and differentiating, we obtain,

$$I = \omega C V_0 \sin (\omega t + \pi/2)$$

$$I = V_0 \sin (\omega t + \pi/2) / X_C$$

where $X_C = (\omega C)^{-1}$ is known as the capacitive reactance.

Here we find that the phase angle is $\pi/2$, implying that the current leads the potential by 90^0 or $\pi/2$ in the case of a pure capacitor.

Similarly, for a circuit element containing a pure inductance, the potential leads the current by 90^0 or $\pi/2$.

Equivalent circuit of an electrochemical cell:

In general, an electrode | solution interface can be considered as an impedance to a small sinusoidal excitation. The impedance of such as a kind of electrochemical interface is a complex number, $Z(\omega)$ that can be expressed either in polar coordinates or in Cartesian coordinates, which are given as follows.

$$Z(\omega) = |Z|\, e^{j\phi}$$

$$Z(\omega) = Z'(\omega) + j\, Z''(\omega)$$

$$Z(\omega) = (Re\ Z)^2 + (Im\ Z)^2$$

where $Z'(\omega)$ and $Z''(\omega)$ are the real (Re Z) and imaginary (Im Z) parts of the impedance and the relationship between these quantities is given by,

$$|Z|^2 = (Z')^2 + (Z'')^2$$

The phase angle ϕ can be expressed as,

$$\phi = Arc\ \tan(Im\ Z\ /\ Re\ Z)\ or\ Arc\ \tan(Z''(\omega)\ /\ Z'(\omega))$$

$$and\quad Re\ Z\ or\ Z'(\omega) = |Z|\cos\phi$$

$$Im\ Z\ or\ Z''(\omega) = |Z|\sin\phi$$

Hence the electrode | electrolyte interface of the electrochemical cell can be represented by a suitable equivalent circuit consists of resistors and capacitors that pass current with the same amplitude and the same phase angle under a given excitation. A typical equivalent circuit for an electrochemical system is shown in the following figure.
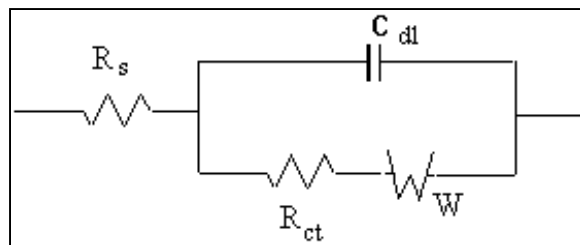

Figure5: Randles equivalent circuit for an electrode reaction

In figure 5, an equivalent circuit popularly known as Randles equivalent circuit [11] for a diffusion controlled electron transfer reaction is shown with the double layer capacitance C_{dl}, the charge transfer resistance, R_{ct}, the Warburg impedance W and the solution resistance, R_s.

The total current of the working electrode is obtained by the sum of distinct contributions from the faradaic current I_f and the double layer charging current I_c. The double layer capacitance arises from the charges stored at the interface between an electrode and its surrounding electrolyte. The charges in the electrode are separated from the charges of the bulk ions. In many cases, the double layer capacitance closely resembles a pure capacitance and hence it is represented by the element C_{dl} in the equivalent circuit. The faradaic impedance Z_f can be separated into two components namely, the charge transfer resistance, R_{ct} and the Warburg impedance, Z_W. The charge transfer resistance, R_{ct} denotes a resistance offered to the electron transfer process and Z_W also represents a kind of resistance to the mass transfer process because of diffusion. This impedance depends on the frequency of the perturbation in terms of the applied potential. At high frequencies, the Warburg impedance is small because the reactants do not have to diffuse very far. In contrast, at low frequencies, the diffusing reactants have to move very far, thereby increasing the Warburg impedance. The uncompensated solution resistance denoted by R_s exists between the working electrode and the reference electrode. In the equivalent circuit representation, the uncompensated solution resistance, R_s is inserted as a series element because all the current must pass through it. In contrast to R_s and C_{dl}, which are nearly ideal circuit elements, the components of faradaic impedance, Z_f namely the charge transfer resistance, R_{ct} and Warburg impedance, Z_W are not ideal because they change with the frequency ω.

For a planar diffusion, the value of R_{ct} can be expressed as,

$$R_{ct} = RT / nFI_0$$

where I_0 is the exchange current density.

The solution resistance R_s is given by the following expression,

$$R_s = x / \kappa A$$

where x is the distance of the capillary tip from the electrode

     κ is the conductivity of the solution

     A is the area of the electrode

The relative values of R_{ct} and Z_W at a given frequency are the measure of the balance between kinetic and diffusion control. If the exchange current density I_0 is very large, then R_{ct} will tend to zero and its value will be too small to measure so that only the Warburg impedance will be observed. On the other hand for a very sluggish electrochemical reaction, R_{ct} will be a dominant term and its value will be very high. The analysis of equivalent circuit and determination of the individual components of it was originated from a long procedure used in electrical engineering. It was first applied to electrochemical applications by Sluyters [12] and it is commonly known as *Complex plane impedance analysis*. A full analysis of these series and parallel combination of elements known as the Randles equivalent circuit has two limiting cases. At low frequencies, as $\omega \rightarrow 0$, the real and imaginary parts of impedance are given by,

$$Z' = R_s + R_{ct} + \sigma\, \omega^{-1/2}$$

$$Z'' = \sigma\, \omega^{-1/2} + 2\, \sigma^2\, C_{dl}$$

where, $\sigma = (RT / \sqrt{2}\, n^2\, F^2\, A\, D^{1/2}\,)\, \{\, 1 / C^{\infty}_0 + 1 / C^{\infty}_R\}$

in which,   D is the diffusion coefficient of the species in solution

        A is the area of the electrode

C^{∞}_0 and C^{∞}_R are the bulk concentrations of the oxidized and reduced species.

On rearranging these equations, we get,

$$Z'' = Z' - R_s - R_{ct} + 2\,\sigma^2\,C_{dl}$$

This is the equation of a straight line of unit slope and with an intercept on the real Z' axis given by, $\quad R_s + R_{ct} - 2\,\sigma^2\,C_{dl}$

At high frequencies where the Warburg impedance is negligible in comparison to R_{ct}, the two components are represented by,

$$Z' = R_s + R_{ct} / (1 + \omega^2\,R_{ct}^2\,C_{dl}^2)$$

$$\text{and} \quad Z'' = C_{dl}\,R_{ct}^2\,\omega / (1 + \omega^2\,R_{ct}^2\,C_{dl}^2)$$

Eliminating ω using these two equations gives,

$$(Z' - R_s - R_{ct}/2)^2 + (Z'')^2 = (R_{ct}/2)^2$$

which is the equation of a circle with center at $Z' = R_s + R_{ct}/2$ and a radius of $R_{ct}/2$.

A plot of the whole expression for Z' verses Z'' for a kinetically controlled reaction is shown in the figure 6.
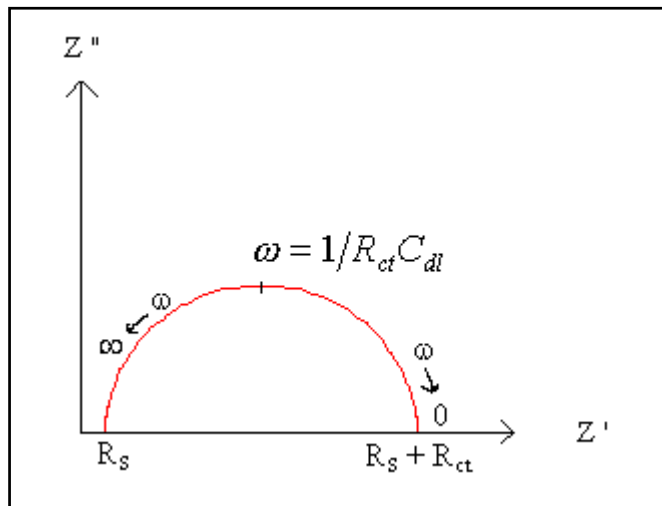

Figure 6: Cole-Cole plot

The Cole-Cole plot of a charge transfer controlled reaction shows a semicircle and it is obtained by plotting the values of Z' and Z'' at different frequencies. It is also known as the Nyquist plot. At infinite frequency, Z'' approaches zero as the capacitance in the equivalent circuit offers a very little impedance. At low frequencies, the impedance is purely resistive, because the reactance of C is very large. The solution resistance has the effect of translating the semicircle on the Z' axis. R_s can be determined by reading out the real axis value at the high frequency intercept. C_{dl} can be obtained from the maximum value of Z'' in the semicircular region where $\omega = 1/R_{ct}C_{dl}$. The diameter of the semicircle provides the value of R_{ct}. Another way of representing the impedance data is by the Bode plot [13]. In this, both the logarithm of the modulus of impedance (log $|Z|$) and the phase angle ϕ are plotted in the y-axis against a common abscissa of frequency (in logarithmic scale). On such a plot a pure resistance is denoted by a horizontal line and a constant phase angle ϕ of 0^0, while a capacitor is a straight line of slope -1 and a constant phase angle ϕ of -90^0. The Bode plots for the Randles equivalent circuit without the Warburg impedance is shown in figure 7.

Figure 7 shows two different kinds of representations of Bode plots. The first one is known as the Bode frequency plot and the other one is called as the Bode phase angle plot. The transition between the horizontal line and the sloping portion in the Bode frequency plot is called a corner and the frequency of intersection of lines extrapolating the straight-line sections is known as the corner frequency. The transitions between asymptotic values indicate the frequency regions where the ohmic and capacitive components have comparable values and neither of them is completely predominant. When the

70

electrochemical system possesses more than one time constant, both the Bode plots and Cole-Cole plot exhibit the characteristic features.
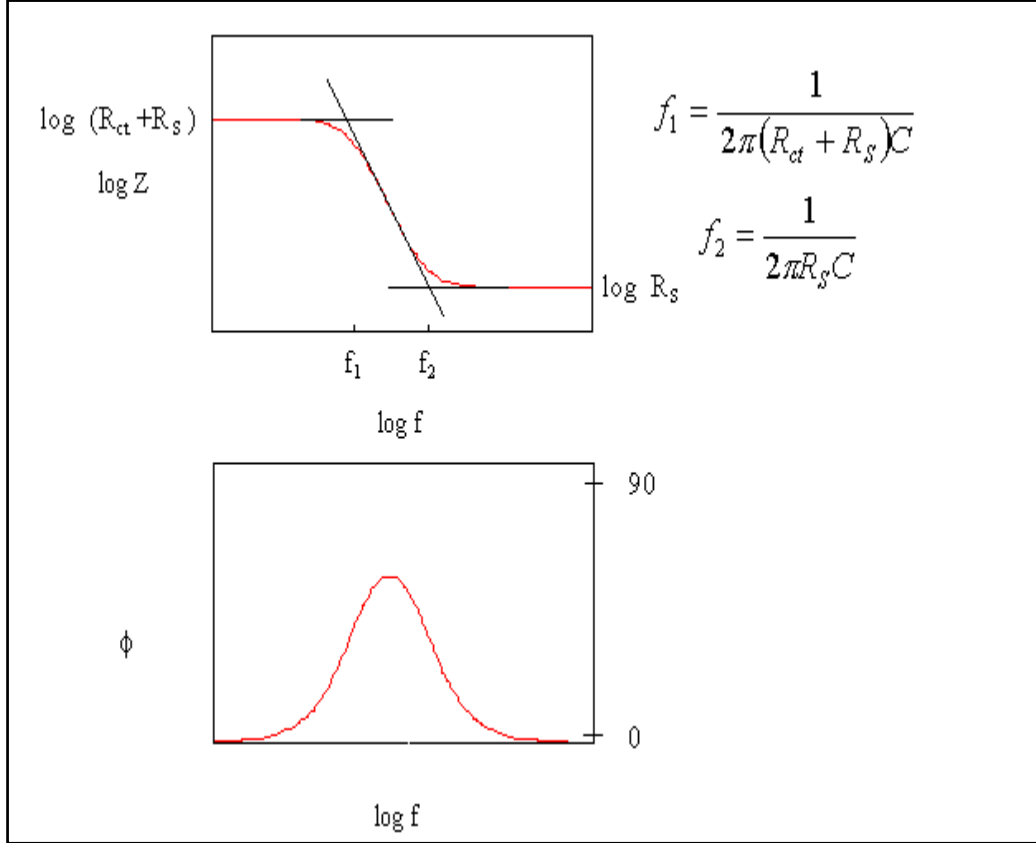

$$f_1 = \frac{1}{2\pi(R_{ct} + R_S)C}$$

$$f_2 = \frac{1}{2\pi R_S C}$$

Figure 7: Bode plots

Measurement of Impedance

The impedance measurements must be made over a wide range of frequency in order to attain the high frequency limit of the impedance equal to the electrolyte resistance. At high frequencies, the capacitive effect is attributed to a pure double layer capacitance. Normally the frequency range used for the measurement is from 100mHz to 10 MHz, depending on the electrochemical system employed for the analysis. There are different types of methods used to measure the impedance of an electrochemical system namely, Wheatstone

bridge, Analogue ac analyzer, Phase sensitive detection, Sine wave correlation, Frequency response analyzer and Fourier transform methods [7,8]. In our work, we have carried out the impedance measurements using a Perkin Elmer Model 5210 lock-in amplifier controlled by PowerSine software. In this case, Phase sensitive detection method [8] was employed to measure the impedance of an electrochemical cell above 5Hz using a Single-sine technique that provides the highest accuracy. Below 5Hz, the measurement of impedance was performed using a fast Fourier transform technique based on multi sine experiments that avoids any drift or change in the impedance value of the electrochemical system. The potential of the working electrode is held at a desired potential of interest using a potentiostat. A small amplitude of sinusoidal ac voltage with 5-10 mV peak-to-peak is applied to the cell from a lock-in amplifier. The current output from the cell has a phase difference with respect to the input voltage. The lock-in amplifier measures this phase difference and amplitude of the current response. Figure 8 shows the principle of working of a phase sensitive detector.

The elements of an equivalent circuit model represent the various macroscopic processes involved in the transport of mass and charge in the electrochemical system. The dispersion relations with the frequency for most of the circuit elements are very simple. If the dispersion diagrams show distinct features that can be easily related to specific physical processes and can be defined to different sub-circuits of the equivalent circuit, then the analysis becomes quite simple. However, if the time constants associated with different sub-circuits are relatively close to each other on the time axis or if the elements with fractional power dependence (<1) on frequency are present (For example, Warburg impedance or a Constant Phase Element (CPE)), then the dispersion curves become convoluted. In these cases, a more sophisticated method of

analysis is required as the variation of one circuit element can affect a large part of frequency dispersion and hence affects the parameters of the other sub-circuits. To overcome this problem, Non-Linear Least Square Fit (NLLSF) technique is used, where all the parameters of the equivalent circuit are adjusted simultaneously. Using this technique, one can obtain the optimum fit to the measured dispersion data and a thorough treatment of this procedure to the electrochemical system was done by Bevington [14].
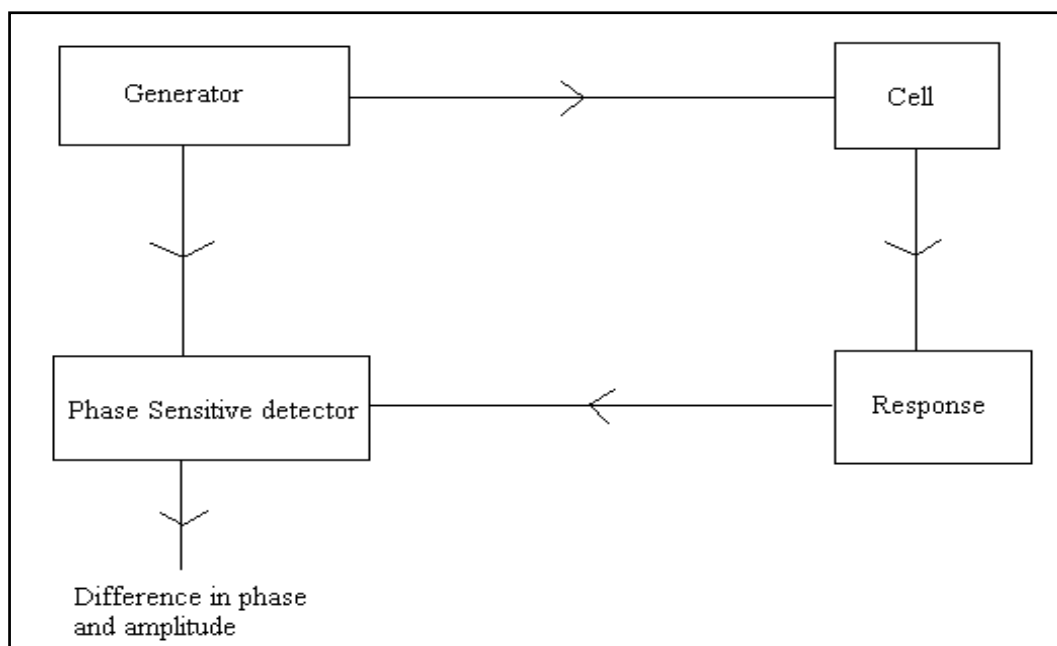

Figure 8: Schematic diagram of a Phase Sensitive Detector

In this work, we have extensively used impedance spectroscopy to study the electron transfer reactions on the SAM modified surfaces, to characterize the template electrodeposited materials and to evaluate the supercapacitors. The measured impedance data were analyzed using the Boukamp's impedance software [15] by fitting to an appropriate equivalent circuit, which can significantly explain the processes occurring at the electrode |

73

electrolyte interface. This software was written by Bernard A. Boukamp in Turbo Pascal (version 3.0) programming language. The impedance data were also analyzed using the ZsimpWin EIS data analysis software provided by Perkin Elmer (version 2.0).

2.7.5. Chronopotentiometry

In this type of experiment, the current flowing through the cell is instantaneously stepped from zero to some finite value and the potential of the working electrode is monitored as a function of time. Overall the rate of the reaction is fixed. This technique comes under the galvanostatic (constant current density) experiment. The plot of potential versus time is known as chronopotentiogram. Figure 9 shows a typical chronopotentiogram for a reversible system.
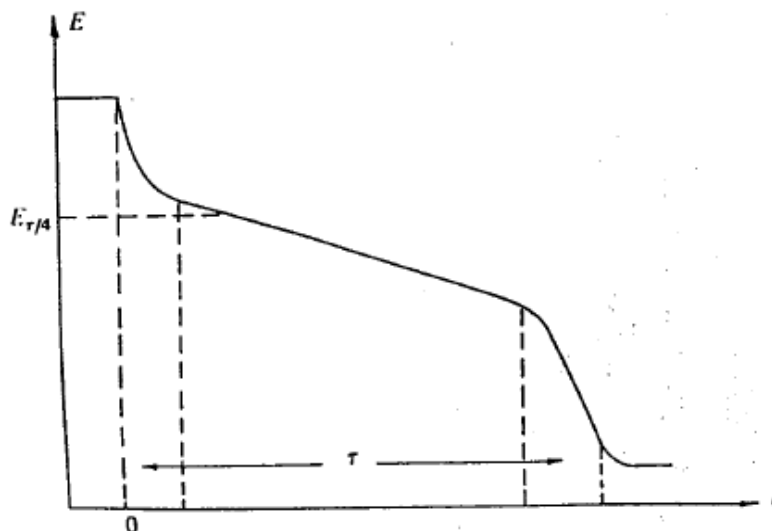

Figure 9: Schematic diagram of a chronopotentiogram for a reversible system

Consider a simple reaction, $O + ne^- \rightleftharpoons R$. As the current pulse is applied there is an initial fairly sharp decrease in the potential as the double

74

layer capacitance is charged, until a potential at which the species O is reduced to R is reached. Then there is a slow decrease in the potential determined by the Nernst equation, until the surface concentration of O essentially reaches zero. The flux of O to the surface is then no longer sufficient to maintain the applied the current and the electrode potential again falls sharply, until a further electrode process occurs. The dependence of current density on the transition time and the diffusion coefficient of the species in this case are given by Sand equation, which is represented as follows.

$$| I\tau^{1/2} | = n \, F \, D_0^{1/2} \, \pi^{1/2} \, C_0^{\infty} / 2$$

where τ is the transition time and D_0 is the diffusion coefficient of the species. Thus the product of $I\tau^{1/2}$ is independent of the applied current density and proportional to C_0^{∞}. This is used as a diagnostic test for a diffusion controlled process. In our work, we have used chronopotentiometry to monitor the change of potential during the galvanostatic template electrodeposition of nickel.

2.7.6. Chronoamperometry

This method comes under the potential step experiment, where the potential of the working electrode is changed instantaneously and the current-time response is recorded. The plot of change of current with time at a constant potential is known as the chronoamperogram and the technique is called as the chronoamperometry. Figure 10 shows the typical potential step applied to an electrochemical system and its response in terms of current that is being recorded as a function of time.
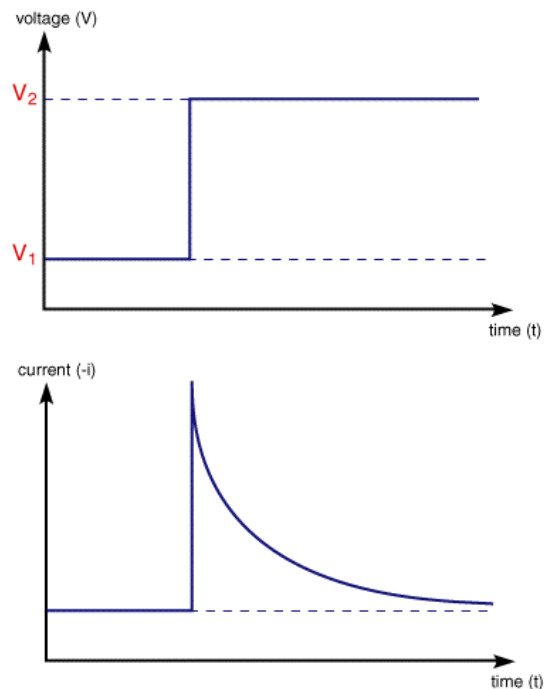
Figure 10: Schematic representation of potential step applied during chronoamperometric measurements and its response in terms of current as a function of time.

It can be seen from the figure that as soon as the potential is applied to an electrochemical system, there is a large flow of current due to the reaction occurring at the electrode surface. Initially the electrode surface is covered fully with the oxidant species and once the potential is applied to the electrode, the formation of reductant species occurs, which results in a large current flow. Further, this current decreases with time due to its dependence on concentration gradient. In our work, we have used this technique to evaluate the high surface area porous nickel obtained from template electrodeposition as a hydrogen evolving cathode as explained in detail in chapter 6.

2.7.7. Tafel plot analysis

Under steady state conditions, when the electron transfer process is irreversible, i.e. when current flows the electron transfer is insufficiently fast to maintain Nernstian equilibrium at the electrode surface, the kinetic data in such cases can be directly obtained from the steady state current-voltage measurements. The analysis is based on the Tafel equations, which are given as follows.

For a cathodic reaction,

$$\log |I| = \log I_0 - \alpha_C \, n \, F \, \eta \, / \, 2.303 \, RT$$

while for an anodic reaction,

$$\log |I| = \log I_0 + \alpha_A \, n \, F \, \eta \, / \, 2.303 \, RT$$

where I is the total current density, I_0 is the exchange current density, α_C and α_A are the respective cathodic and anodic Tafel slopes and η is the overpotential, which is defined as the deviation of applied potential from the equilibrium potential. Generally the Tafel approximation is used for $|\eta| \geq 70/n$ mV. The plot of log |I| versus η is known as the Tafel plot, from which the values of α_C, α_A and exchange current density (I_0) can be determined from the slopes and intercept respectively. The Tafel plot analysis is extensively used in the corrosion studies and catalysis especially for hydrogen evolving cathodes. In our work we have used Tafel plot analysis to study the hydrogen evolution reaction (her) on the porous nickel surface, thereby evaluating it as a hydrogen-evolving cathode in catalysis.

2.7.8. Grazing angle FTIR spectroscopy

Fourier transform infrared spectroscopy, popularly known as FT-IR spectroscopy is mainly based on the interaction of infrared (IR) radiation with a sample (liquid or solid) and measuring the frequencies at which the sample absorbs the radiation. The FTIR spectrometer records the intensities of absorption over a range of frequency and represented in a two-dimensional plot called IR spectrum. Intensity is generally reported in terms of absorbance, the amount of light absorbed by a sample, or percentage of transmittance, the amount of light that passes through the sample. The frequency is expressed in terms of wave numbers. The key components of a FTIR spectrometer are the source, the interferometer and the detector. The interferometer provides a means for the spectrometer to measure all the optical frequencies simultaneously by modulating the intensity of individual frequencies of radiation before the detector picks up the signal. The output of an interferometer after scanning over the frequency range is known as an interferogram, which is a plot of intensity versus the mirror position. Using the mathematical process of Fourier Transform (FT), a computer converts this interferogram into a spectrum, which is the final output from the FTIR spectrometer. The chemical structure and the presence of various functional groups in the given sample can be identified from this spectrum, as the chemical functional groups absorb IR radiation only at certain particular frequencies.

In addition to bulk samples, FTIR can be used in surface science mainly to study ultra thin organic films on various metallic and non-metallic surfaces essentially to characterize the molecular packing and orientation on the surface [16,17]. The spectrum is obtained using either internal or external reflection modes of operation. The internal reflection mode is known as the (ATR) Attenuated Total Reflection spectroscopy, whereas the external

reflection mode is known as Reflection-Absorption or Grazing Angle spectroscopy. Attenuated Total Reflection (ATR) is a multiple internal reflectance technique, which has been explained in detail by Griffiths et al. [18]. The beam is directed into an angled crystal and reflected within the crystal until it emerges from the other end where it has been collected. The number of reflections depends on the angle of incidence upon the crystal. The crystal is usually made of KRS-5, Zinc selenide or Germanium. Grazing Angle Reflection or External Reflection technique provides a nondestructive method of measuring the surface coatings of thin films. External reflectance is a mirror like reflection from the surface of a sample. The infrared radiation is directed onto the surface of a sample at an angle of incidence θ_I. For an external reflectance, the angle of reflection, θ_R, is equal to the angle of incidence, θ_I. The amount of radiation reflected from the sample depends on the angle of incidence, refractive index, surface roughness and the absorption properties of the sample. The angle of incidence is selected on basis of the thickness of coating, which is being used for the study. For very thin film coatings in the range of nanometer thickness like ultra thin organic films, an angle of incidence of 85^0-88^0 is used for the characterization of modified surfaces. Reflectance measurements at this angle of incidence are often called as grazing angle measurements. For samples with the coatings of micrometer thickness range, a 30^0 angle of incidence is normally chosen for the measurement. The reflection-absorption spectrum for a monolayer of organic molecules adsorbed onto a metal surface is measured mostly at a higher angle of incidence. In these cases, the measurements are mainly based on the p-polarization component of the incident light, which alone is allowed to pass through the sample surface [19]. The p-polarization component of the incident light has its orientation parallel to the plane of incidence. On the other hand, the s- polarization component of the

incident light has its orientation perpendicular to the plane of incidence. Hence the s-polarization component of the incident light does not interact with ultra thin film samples on metal surface and therefore does not contribute to any spectral signal. It is clear that the Grazing angle FTIR spectra obtained in the case of monolayer modified surfaces are due to the interaction of only p-polarized light, which results in very high quality and clear spectra. The spectrum of an ultra thin organic film modified metal substrate is obtained by the ratio of the absorbance spectrum of the monolayer-coated surface with a suitable blank spectrum (taken on a bare substrate). The relative intensities of the absorption peaks in the spectrum are affected mainly by the average orientation of transition dipoles relative to the surface. A transition dipole parallel to the metal surface will exhibit a greatly attenuated peak in intensity relative to the transition dipole perpendicular to the metal surface. From this analysis, the average orientation of the monolayer chains and the terminal groups can be obtained. The peak positions in the spectra also provide information about the dynamic behaviour and the state (for example the crystalline like, liquid like) of the monolayer.

In our work, we have carried out the FTIR spectroscopy studies for the SAM modified surfaces using a FTIR 8400 model (SHIMADZU) with a fixed 85^0 grazing angle attachment (FT-85; Thermo Spectra-Tech). The FT-85 grazing angle attachment does not use the mirror like conventional reflectance accessories. Instead, it uses silicon refracting optical elements with the existing beam diverge in the sample compartment to obtain a high, 85^0 angle of incidence. The unique design of the FT-85 also features the built-in polarizing elements. The silicon refracting elements are positioned at angles, which allow only the p-polarization light to pass through the sample. The samples are placed on the horizontal sampling surface of the accessory. Therefore, no clamps are

necessary. The sample area is approximately 10 mm wide and 40-50 mm long. The FT-85 accessory is available for almost all the popular FTIR spectrometers and is easily installed with minimal alignment. The accessory is mounted on a base-plate to ensure the reproducibility. The typical diagram of the FT-85 accessory used in our grazing angle FTIR spectroscopy studies is shown in the figure 11.

Figure 11: FT-85 accessory used for the grazing angle FTIR spectroscopy

2.7.9. X-ray diffraction

X-ray diffraction (XRD) is a non-destructive technique for the qualitative and quantitative analysis of the crystalline materials, in form of either powder or solid. Basically XRD is obtained as the "reflection" of an X-ray beam from a family of parallel and equally spaced atomic planes, on the basis of Bragg's law [20]. Diffraction occurs as the waves interact with a regular structure whose repeat distance is about the same as the wavelength. The phenomenon is common in the natural world and occurs across a broad range of scales. For example, light can be diffracted by a grating having scribed lines spaced on the order of a few thousand angstroms, about the wavelength of light. It happens that X-rays have wavelengths on the order of a few angstroms, the

same as typical interatomic distances in crystalline solids. That means X-rays can be diffracted from minerals, which are crystalline and have regularly repeating atomic structures.

In 1912, W.L. Bragg recognized that when certain geometric requirements are met, X-rays scattered from a crystalline solid could constructively interfere to produce a diffracted beam and has given a relationship based on the several factors known as the Bragg's law. The schematic representation of this law is shown in the following figure.
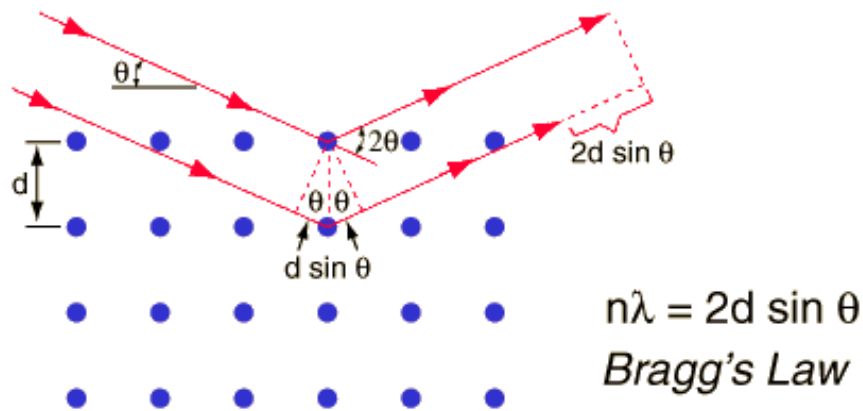

Figure 12: Schematic representation of Bragg's law

When a monochromatic X-ray beam of wavelength λ is incident on lattice planes with an angle θ, the diffraction occurs if the path of rays reflected by successive planes (with a distance 'd') is a multiple of the wavelength. Then it is possible to analyze the 'd' spacing of a crystal (or a powder) by measuring the first-order angles of diffraction, using the formula,

$$d = n \, \lambda \, / \, 2 \sin \theta$$

where, n is an integer, λ is the wavelength of X-rays in angstroms, d is the interatomic spacing in angstroms and θ is the diffraction angle in degrees. The wavelength of X-ray used for the analysis is 1.54 Å. X-rays with wavelength on the order of lattice spacing are elastically scattered (diffracted) from the atomic

planes in a crystalline material yielding the diffraction peaks. The plot of intensity of X-ray with the diffraction angle (2θ) is known as the diffractogram. The qualitative analysis of the diffractogram obtained from the specimen can be done by comparing with a huge number of diffraction patterns available in the official database. Single phases and/or mixtures of phases can be analyzed with the programs available today.

X-ray diffraction technique is widely used to identify the unknown crystalline phase, determine the residual stress, microstrain, preferred orientation and crystallite size or grain size and also in structural analysis of the specimen. Apart from this, XRD can also be used in the study of thin films to investigate the properties of the multilayer, by keeping the incident beam at very low angles thereby minimizing the interference due to the substrate, as the same way reflectometry can be performed. In our studies, we have used XRD essentially to investigate the different liquid crystalline phases formed by the self assembly of surfactants and to determine the crystallographic orientation and grain size of the template deposited materials.

2.7.10. Scanning Electron Microscopy (SEM)

SEM comes under the category of electron microscopes, which were developed due to the limitations associated with the light microscopes such as the magnification and resolution. The electron microscopes are scientific instruments that use a beam of highly energetic electrons to image the specimen on a very fine scale and to gain information on its structure and composition. The analysis of images obtained form the electron microscope can provide information on the topography, morphology, composition and the crystallographic orientation of the sample. There are two kinds of electron microscope namely Transmission electron microscope (TEM) and Scanning

electron microscope (SEM) that are commonly used in the surface science. In our work, we have used SEM to characterize the surface morphology of the electrodeposited materials.

The first Scanning electron microscope (SEM) was introduced in the year 1942 to study the structural aspects of the surface on a very fine scale. SEM uses the electron beam rather than light to form an image. The electromagnets are used to bend the electron beam to produce the image on a screen. By using the electromagnets, we can have more control over the magnification and the use of electron beam provides a greater clarity in the image produced. There are many advantages of using the SEM instead of a light microscope. The SEM has a large depth of field, which allows a large amount of the sample to be in focus at one time. The SEM also produces images of high resolution, which means that closely spaced features can be examined at a very high magnification. The combination of higher magnification, larger depth of focus, greater resolution, and ease of sample preparation makes the SEM one of the most extensively used instruments in research areas today.

A beam of electrons is generated from the electron gun using tungsten tip located at the top of the column. This beam is attracted through the anode, condensed by a magnetic lens and focused as a very fine point on the sample by the objective lens. The scan coils are energized (by varying the voltage produced by the scan generator) and create a magnetic field, which deflects the beam back and forth in a controlled pattern. Once the beam hits the sample surface there are many possibilities that can occur by the interaction of electron beam with the surface, which are shown in the figure 13. As for as the SEM is concerned, when the electron beam hits the sample surface, the secondary electrons produced from the sample are collected by the secondary electron

detector or the backscatter detector, which has been converted into a signal resulting in an image in the viewing screen. The image obtained corresponds to the surface topography of the sample. When a SEM is used, the column must always be in a vacuum. This avoids the problem of interaction of electron beam with the other gaseous molecules, which would result in the lower contrast images. A very important point in the study of SEM is that the sample should be conductive and for this reason a thin film of gold is coated over the sample surface using sputtering technique before the process of imaging.
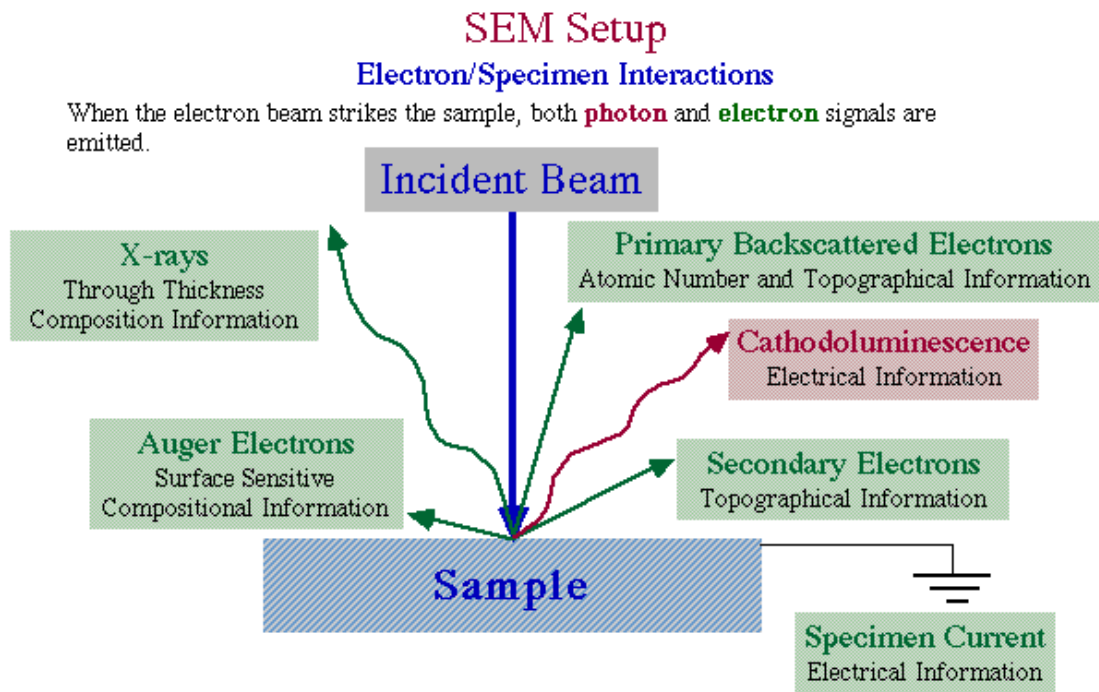

Figure 13: Schematic representation of electron beam-specimen interactions

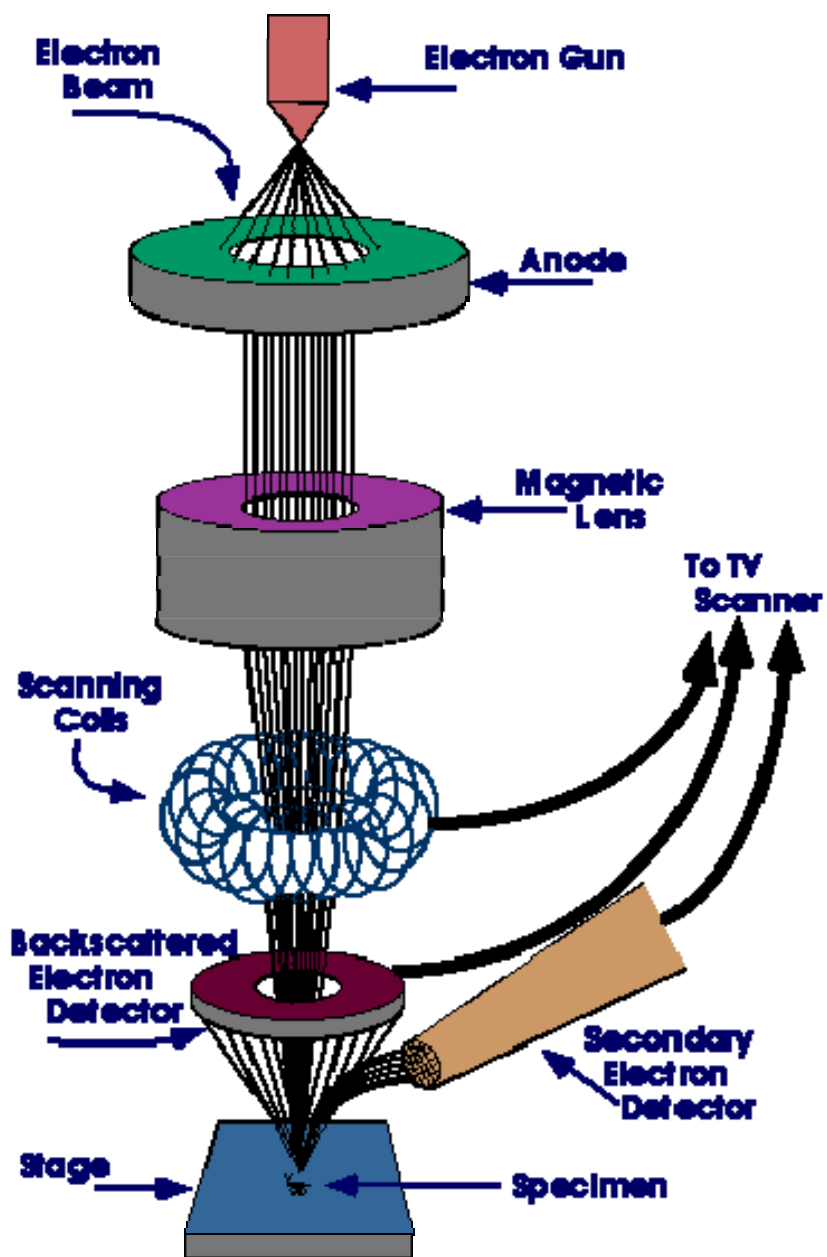The working principle of a scanning electron microscope is schematically shown in the following figure 14.

Figure 14: Schematic representation of the working principle of a SEM

In our work, we have used SEM to study the structural morphology of the template electrodeposited materials and their characterization. The typical picture of the SEM that we have used in our work is shown in the following figure 15.

Figure 15: Picture of a Scanning Electron Microscope (SEM)

2.7.11. Scanning Tunneling Microscopy (STM)

The Scanning Tunneling Microscopy (STM) [21] is a versatile tool to obtain the topographic images of smooth conductive surfaces in the area of surface science. The instrument scanning tunneling microscope was invented by Gerd Binnig and Heinrich Rohrer [22] at the IBM research institute, Zurich in the year 1982 for that they obtained the noble prize in 1985. It can be used in the investigation of very small areas of surfaces in the order of nanometers with extremely high level of precision. It also has the advantage of studying atomically smooth conducting surfaces in a variety of environments like ultra high vacuum (UHV), air, electrolytic media etc. In a typical STM experiment an atomically sharp metallic tip made up of either Pt/Ir, Pt/Rh, Pt or W is

brought very close to the surface with the separation of the order of few angstroms between them. The movement of the tip in all the three direction is carried out with the help of piezoelectric crystals. Application of a small potential difference (~0.1V) between the sample surface and the tip leads to the flow of tunneling current in the order of pA to nA [23]. This tunneling is due to the fact that the electron wave functions of the tip and the sample overlap. The tunneling current is of the form $I_t \approx V\ e^{-kd}$ where I_t is the tunneling current, V is the bias voltage, k is a constant that includes the work function of the material and d is the spacing between the lowest atom on the tip and the highest atom on the sample. The strong exponential dependence of the tunneling current on the tip-to-sample spacing makes it possible to use this current in a feedback loop to control the motion of the tip precisely using a device known as the piezoelectric scanner. In response to an applied voltage, the scanner moves the tip over an area of the sample in a raster pattern and the feedback loop causes the tip to track the sample surface with sub-angstrom precision. The coordinates of the tip's path can then be transformed into a map of the surface topography. In fact, the STM image at atomic resolution corresponds to a contour map of the local density of states (LDOS) of atoms on a conducting sample. The tunneling current is very much sensitive to the distance between the tip and sample. This current decreases about one order of magnitude per 1Å of the electrical gap width, which results in an accuracy of the order of 0.1Å that can be achieved using STM. This extreme sensitivity of the STM means that the features, which are of atomic dimensions, can be imaged precisely provided the distance between the tip and the sample is accurately controlled.

The STM can be operated in two ways namely the constant current mode and the constant height mode. In the constant current mode of operation, the tip is moved slowly in the y-z plane, which is parallel to the sample surface

and simultaneously the distance x from the sample surface (height) is adjusted in such a way that the current will remain constant by the application of a feedback voltage to the tip. The image is obtained as a map of this feedback voltage versus the lateral y & z coordinates resulting in the topographic image of the surface. In this way the structure of single crystal surfaces, the occurrence of steps, kinks and defects can be realized. In the constant height mode, the tip is moved at a constant height x from the sample to image the surface. As a result, the tunneling current will change as a change of tip-sample separation. In this case, the current is recorded as a function of lateral coordinates to obtain the topographic image of the sample. This technique is generally used on atomically smooth conducting surfaces only, since on rougher surfaces the tip may hit a protrusion leading to tip crash that results in blurred images. In our work, we have carried out STM studies extensively on the modified surfaces using a home built instrument [24,25].

Brief description on the principle and design of STM

The designing and fabrication of the STM involve several important factors such as efficient vibration isolation, minimum thermal drift, proper feedback control, preparation of atomically sharp tunneling tips and coarse positioning of the tip. Since the tunneling current is in the order of nA to pA, the measurement of such a small current and obtaining a good resolution STM image requires vibration free environment. This can be achieved by increasing the resonance frequency of the STM scan unit such as using the tube piezo scanners, which can eliminate both the external and internal low frequency vibrations. The rigidity of the scan unit is one of the important factors in the vibration isolation system. It is mounted inside a nylon block with a hole and is secured by two screws to a cylindrical PVC block. The whole assembly is

screwed onto a thick brass plate and is mounted onto a stack of three more brass plates each separated by a viton O-ring. The entire assembly is suspended using a bungee chords to the ceiling to damp the low frequency vibrations. The thermal drift during the measurement is compensated by the proper selection of materials and symmetric design of scan unit.

Very sharp tips having typically one atom at the edge can be prepared by electrochemical etching of inert metal wires such as W, Pt-Rh or Pt-Ir. The Pt-Rh wire of 0.25 mm diameter is etched using an ac voltage in an electrolytic solution containing 5% NaCl and 5% NaNO$_3$, whereas the W tips are prepared by etching in 5% KOH solution. The tip obtained by this method is dipped in HF solution to remove any surface oxide, rinsed in distilled water and dried before using as a probe for the measurement in STM.

The coarse positioning is achieved using inertial sliding mechanism, based on the infinitesimal horizontal motion of the sample stage relative to its starting position when a suitable saw tooth waveform is applied. This is because the large acceleration provides enough inertial forces that exceed static friction during the falling portion of the saw tooth waveform, while during the slow rise of the waveform the sample stage essentially follows the motion of the piezo. The scan unit is built up of two concentric piezo electric tubes, the inner one for scanning the tip and the outer one for moving the sample holder towards or away from the tip. The piezo tubes are coated with silver on both outside and inside of the tube. The inner piezo tube holds the tip coaxially. The coarse positioning is achieved by applying a saw tooth waveform to the outer piezo tube, while the metallized inside portion of the tube is grounded. This will compress the tube and as a result the glass tube containing the sample holder is being brought closer to the tip. During the falling portion of the saw tooth waveform and during the sudden release of the tube, the glass tube attached to

the piezo quickly retracts, while the sample holder can not retracts due to the inertial forces. As a result, the sample holder is being translated towards the tip by one step. By applying a train of saw tooth pulses of about 120V amplitude and fast scan rate, speeds of about 1 mm/s both towards and away from the tip can be achieved. The following diagram shows the schematic representation of working principle of a STM.
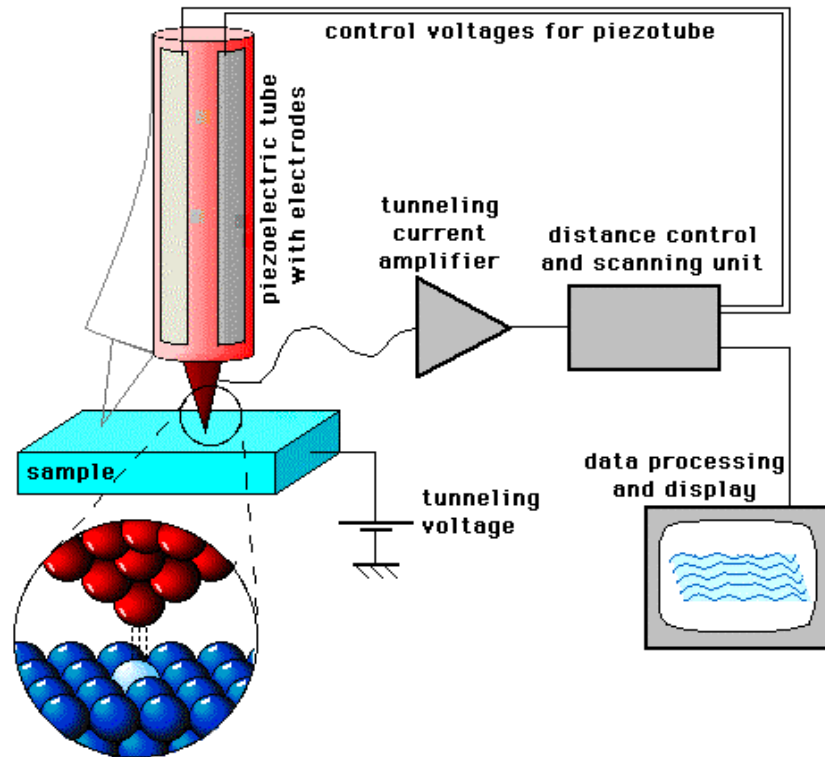

Figure 16: Schematic diagram of working principle of a STM

As mentioned earlier, the STM can be operated either in constant current mode or in constant height mode. In the constant current mode of operation, the tip is scanned over the sample surface in such a way that the gap separation is always maintained constant at a reference value, by the application of a feedback voltage to the inner piezo. The feedback voltage needed for

maintaining the tunneling current constant is a measure of the surface topographical image. For constant current mode, the feedback control unit plays a very important role. The feedback control unit compares the actual tunneling current with the user specified reference current. When the measured current is very large, the feedback control unit generates a voltage, which is applied to the piezo tube scanner to pull the tip back from the sample and vice versa. The piezo tube expands linearly with the applied voltage, which is directly proportional to the changes in the vertical tip position. In the constant height mode the tip is scanned over the sample in the same plane by keeping the gap separation constant, resulting in the variation of tip-sample separation depending upon the surface, which in turn changes the tunneling current ultimately.

The electronics involved in the design of the STM mainly consists of the current amplifier, analog feedback system, data acquisition using A/D and the piezo drivers comprising of the D/A card interfaced to a PC and high voltage amplifiers. The current amplifier is a high impedance operational amplifier AD 529, which converts current into voltage over a 10 MΩ metal film resistance. This provides an output voltage of 10 mV for a current of 1 nA. The bias voltage is applied to the sample from the battery through the non-inverting input of the current amplifier. The output of the current amplifier is further amplified by 10 times using an instrumentation amplifier AD 624. An absolute value circuit (AVC) comprising of two low noise OPA 27 op-amps provides the positive voltage to the logarithmic amplifier (AD 759 N). The logarithmic amplifier is used to linearize the exponential behaviour of the current response. A set of five high voltage operational amplifiers (APEX PA42) was used to drive the piezo tubes for coarse positioning and x-y scanning. This amplifier has a maximum voltage of operation of 350 V and output current of 120 mA.

A personal computer interfaced with a Keithley 500A measurement and control system consist of a 16 channel, 16 bit A/D card and two 2 channel, 16 bit D/A cards are used for data acquisition and control. The feedback signal from the integrator is fed to one of the channels of the A/D. Two of the D/A outputs are used for coarse positioning and z control, while the other two are used for x-y scanning. The current amplifier output represents the tunneling current and the logarithmic amplifier output provides the logarithm of the tunneling current that is fed to another two channels of the A/D respectively. The tip scan and the data acquisition proceed concurrently and synchronously. The STM line scan image is displayed in real time. All the images shown in this thesis are raw data images except for plane correction using scanning probe image processor software (Image Metrology, Denmark). Before each experiment the STM is calibrated using atomic resolution images of ZYA grade highly oriented pyrolytic graphite (HOPG) (Advanced Ceramic Co, USA). Figure 17 shows the 2 nm x 2 nm constant current STM image of the above-mentioned HOPG obtained using the home built STM in our laboratory. The hexagonal symmetry pattern of the graphite lattice can be clearly seen from the image.
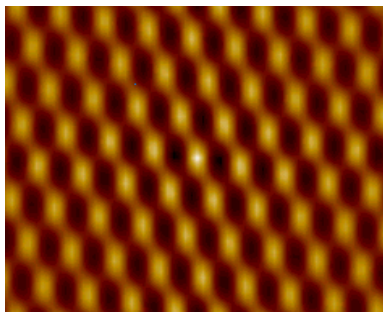

Figure 17: Constant current STM image of HOPG showing the atomic resolution at 2 nm x 2 nm scan range using a bias voltage of 100 mV and I_t of 1 nA

Figure 18 shows the picture of a scanning tunneling microscope that has been fabricated in our laboratory [25] and extensively used for the study of chemically modified surfaces in this work.

Figure 18: Picture of the STM built in Raman Research Institute (RRI)

2.7.12. Polarizing light microscopy (PLM)

Polarized light microscopes have a high degree of sensitivity and can be used for both the qualitative and quantitative analysis of materials that have optical anisotropy. They are designed mainly to observe and photograph the textural changes occur in the anisotropic materials. The working principle of PLM depends on the interaction of plane-polarized light with the anisotropic material and the light reflected from the specimen. For this purpose, the polarizer and analyzer are used. When the electric field vectors of a light wave are restricted to a single plane using the filter known as the polarizer, then the

light is said to be ***polarized*** with respect to the direction of propagation and all waves vibrate in the same plane. The analyzer is oriented perpendicular to the polarizer. That is the polarizer only transmits light that vibrates in one plane and the analyzer transmit light that vibrates in the perpendicular direction. When the analyzer is inserted the light in such a case is said to be cross-polarized. If the light passes from the polarizer to the analyzer without being changed or affected by passing through an anisotropic material then no light will pass through the analyzer because all of the light that reaches it is vibrating parallel to the specimen within the analyzer. When light passes through the anisotropic minerals it splits into two beams that vibrate perpendicular to each other. Because each of these beams travels in different directions in the specimen, they will encounter different resistance to their motion and so will travel at different speeds. The term ***birefringence*** is the difference between the maximum and minimum indices of refraction in an anisotropic material.

When the plane-polarized light is allowed to interact with a birefringent (or doubly-refracting) specimen, two individual wave components that are polarized in mutually perpendicular planes are produced. The velocities of these components are different and vary with the propagation direction through the specimen. After exciting the specimen, the light components become out of phase, but are recombined with constructive and destructive interference when they pass through the analyzer. Polarized light microscopy is a contrast-enhancing technique that improves the quality of the image obtained with birefringent materials when compared to other techniques such as darkfield and brightfield illumination, differential interference contrast, phase contrast, Hoffman modulation contrast, and fluorescence. This technique is mainly used in crystallography, geology, and mineralogical studies. In our studies, we have used polarizing light microscopy to characterize the different

liquid crystalline phases formed by the self-assembly of surfactant molecules using textural analysis. The following figure shows the diagram of a polarizing light microscope used in our work.
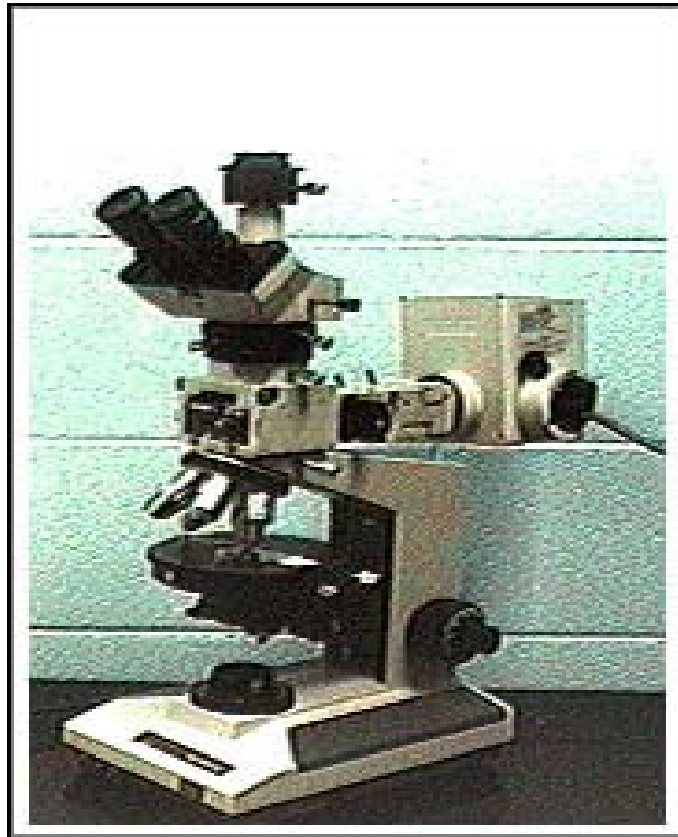

Figure 19: Picture of a polarized light microscope

References:

1. S.E. Creager, L.A. Hockett, G.K. Rowe, *Langmuir*, 8, (1992), 854.

2. E. Boubour, R.B. Lennox, *J. Phys. Chem. B*, 104, (2000), 9004.

3. Y. Golan, L. Margulis, I. Rubinstein, *Surf. Sci.*, 264, (1992), 312.

4. *Modern Electroplating*, by F.A. Lowenheim, Third edition, John Wiley & Sons, New York, (1974).

5. B.E. Conway, J.O.M. Bockris, *Electrochim. Acta*, 3, (1961), 340.

6. W.K. Burton, N. Cabrera, F.C. Frank, *Nature*, 163, (1949), 398.

7. *Electrochemical Methods – Fundamentals and Applications*, by A.J. Bard, L.R. Faulkner, John Wiley & Sons, New York, (1980).

8. *Instrumental methods in Electrochemistry*, by Southampton Electrochemistry Group, Ellis Horwood Limited, (1985).

9. S. Trasatti, O.A. Petrii, *Pure & Appl. Chem.*, 63, (1991), 711.

10. *Comprehensive Treatise of Electrochemistry*, E. Yeager, J.O.M. Bockris, B.E. Conway, S. Sarangapani (Eds), Volume 9, Plenum Press, (1981).

11. J.E.B. Randles, *Disc. Faraday Trans Soc.*, 1, (1947), 11.

12. M. Sluyters-Rehbach, J.H. Sluyters, in *Electroanalytical Chemistry*, by A.J. Bard (Ed), Volume 4, Chapter 1, Marcel Dekker, New York, (1970).

13. B.D. Cahan, C.T. Chen, *J. Electrochem. Soc.*, 129, (1982), 700.

14. P.R. Bevington, in *Data Reduction and Error Analysis for the Physical Sciences*, McGraw-Hill, New York, (1969).

15. B.A. Boukamp, *Equivalent Circuit Software*, Perkin Elmer, Second edition.

16. M.D. Porter, T.B. Bright, D.L. Allara, C.E.D. Chidsey, *J. Am. Chem. Soc.*, 109, (1987), 3559.

17. C.E.D. Chidsey, D.N. Loiacono, *Langmuir*, 6, (1990), 682.

18. *Fourier Transform Infrared Spectroscopy*, by P.R. Griffiths, J. De Haseth, Wiley Inter Science, New York, (1986).

19. J.F. Blanke, S.E. Vincent, J. Overend, *Spectrochim. Acta: Part A*, 32, (1976), 163.

20. *Chemical crystallography: An Introduction to Optical and X-ray methods*, by C.W. Bunn, Second edition, Clarendon Press, Oxford, (1961).

21. *Introduction to Scanning Tunneling Microscope*, by C. Julian Chen, Oxford University Press, New York, 1993.

22. G. Binnig, H. Rohrer, C. Gerber, E. Weibel, *Appl. Phys. Lett.*, 40, (1982), 178.

23. *Scanning Tunneling Microscopy and its applications*, by C. Bai, Springer Series in Surface Science, Volume 32, Springer, Berlin, (1992).

24. V. Lakshminarayanan, *Curr. Sci.*, 74, (1998), 413.

25. M. Jayadevaiah, V. Lakshminarayanan, *Meas. Sci. Technol.*, 15, (2004), N35.